Microwave propagation through an apertured coaxial waveguide

Thomas J. T. Kwan and William Peter
Los Alamos National Laboratory, Los Alamos, New Mexico 87545
(Received 25 January 1988; revised manuscript received 6 June 1988)

We have studied microwave coupling phenomena in linear and nonlinear regimes. Analytic calculations and two-dimensional plasma simulations were carried out for microwave transmission in an apertured coaxial waveguide. In the linear regime, the transmission characteristics for a finite-length aperture that includes the fringing fields were obtained. In the nonlinear regime, where field emission of electrons occurs, we found that the microwave transmission was characterized by the parameter Ω^2/ω^2, where Ω is the electron cyclotron frequency in the electromagnetic field and ω is the microwave frequency. When $\Omega^2/\omega^2 \ll 1$ and $\Omega^2/\omega^2 \gg 1$, significant microwave power can be transmitted through the aperture. For $\Omega^2/\omega^2 \gtrsim 1$, aperture closure due to field-emitted electrons becomes important, and severe degradation of microwave transmission was observed in our simulation.

I. INTRODUCTION

Microwave propagation in structures is an important issue in assessing the performance of pulsed power systems and the vulnerability of objects to ambient high-power microwave radiation. As we might expect, the details of coupling of microwave power inside a system through its antenna and various openings depends on the properties of the incident microwaves and characteristics of the object. This theoretical task is, in general, very difficult because of the complexity of the physical phenomena involved. However, it is important to obtain some general understanding and, in particular, parametric dependence, concerning propagation of microwaves through simple structures. The phenomenon of propagation of microwaves in structures can be divided into linear and nonlinear regimes. In the linear regime, the structures are passive elements and circuit analysis can be used to obtain microwave transmission characteristics. This regime is applicable to the incidence of low-power microwaves on objects. On the other hand, when the microwave power is sufficiently high that electron field emission and air breakdown become important, the structures are active elements in the physics of microwave propagation. This is the nonlinear regime of microwave

We have modeled microwave transmission in a simple configuration using our two-dimensional fully electromagnetic relativistic particle-in-cell code ISIS.[1] An apertured coaxial waveguide (Fig. 1) is used where a TEM wave is input from one end and its transmission through the aperture is monitored. The aperture acts as a generator of all the possible waveguide modes that are either propagating or evanescent. These waveguide modes may be TE or TM modes which carry electromagnetic energy corresponding to their levels of excitation. One of the ways to analyze the linear response of the apertured waveguide to an incoming TEM wave is through the use of an equivalent circuit consisting of lumped circuit elements which are inductors and capacitors. The computer simulation results on the linear response compared favorably with the circuit analysis. The aperture in our calculations could be thought of as an opening of an object. The study of this rather idealized geometry as illustrated in Fig. 1 allows us to gain insight into the dependence of microwave power coupling into physical structures.

II. LINEAR REGIME

The linear regime applies where the microwave power is low and therefore the structure acts in a passive way for the transmission of microwave power. When a TEM wave propagates in the coaxial waveguide as shown in Fig. 1, higher-order modes will be necessarily excited at the aperture to satisfy the electromagnetic boundary conditions there. First of all, it is important to examine the dominant mode in a coaxial waveguide. The transverse electromagnetic mode is the dominant mode for wave transmission in a coaxial waveguide. The dispersion relation is $\omega = kc$. Note that the transmission line is dispersionless, with $v_p = v_g = c$, and that there is no cutoff frequency. However, there also exist higher-order transverse magnetic and transverse electric modes in a coaxial waveguide with cutoff frequencies approximately given by $\omega_{co} = n\pi c/(r_0 - r_i)$ and $\omega_{co} = 2nc/(r_0 + r_i)$, respectively. Here, r_0 and r_i are the outer and inner radii of the

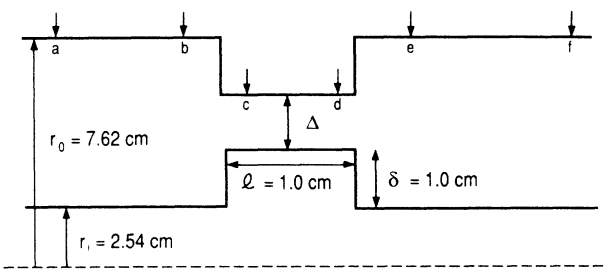

FIG. 1. Schematic drawing of the apertured coaxial waveguide used in the study.

waveguide and $n=1,2,3,\ldots$. We ignore the TE modes, which we are not required to satisfy the boundary conditions at the discontinuity, and further, they are not azimuthal symmetric and, therefore, cannot couple to the TEM waves under our consideration. If $r_0/r_i<3$, the dispersion of the higher-order TM modes can be accurately given by

$$\omega^2 \approx k^2c^2+\left[\frac{n\pi c}{r_0-r_i}\right]^2 . \tag{1}$$

These higher-order modes have cutoff frequencies for propagation and the lowest cutoff frequency is given by $n=1$, $\omega_{co}=\pi c/(r_0-r_i)$. Depending on the frequency of the input TEM wave, higher-order modes can be propagating or evanesent. Specifically, when it is above the cutoff frequency, one will expect the higher-order mode to be propagating with the phase velocity approximately given by[2,3]

$$v_{ph}=\frac{\omega}{k}=c\left[1+\frac{n^2\pi^2}{k^2(r_0-r_i)^2}\right]^{1/2}, \quad n=1,2,3,\ldots . \tag{2}$$

If the input microwave frequency is below the cutoff frequency, the higher-order modes decay away from the aperture since their propagation in the waveguide is not possible. The frequency of the incident microwaves is found to be an important parameter in the transmission characteristics of the aperture shown in Fig. 1. The results indicate that the nature of the higher-order modes in the waveguide plays an important role in microwave power transmission.

The transmission of electromagnetic radiation in a coaxial transmission line with discontinuities was studied extensively for cases where $r_0-r_i<\lambda/2$ (Refs. 4 and 5), and the interference between adjacent discontinuities can be ignored. λ is the wavelength of the TEM wave. Two approaches were used. The coaxial line can be approximately modeled by an equivalent circuit treating the discontinuities as capacitors. In the static field approximation, one can determine the capacitances.[4] Another approach is to represent the electromagnetic fields as a sum of normal modes in the coaxial waveguide and to apply the proper boundary condition at the discontinuities. The ratios of the amplitudes of all higher-order modes to the TEM wave are completely determined by a matrix equation representing an infinite number of simultaneous equations. In practice, of course, one would solve a finite number of equations to yield an approximate solution.

We have used the two-dimensional fully electromagnetic relativistic particle-in-cell simulation code ISIS to study the transmission of microwaves in the apertured waveguide. The advantage of the computer simulation method is to solve the problem dynamically in all regimes. For example, the excited higher-order modes can be above their cutoff frequencies and become propagating in the coaxial transmission line. This is in contrast to the previous treatment which limited the higher-order mode to be nonpropagating and localized in the vicinity of the discontinuity.

A transverse electromagnetic wave was launched from the left-hand side of the waveguide in Fig. 1. The electric and magnetic fields are

$$E_r=-\frac{E_0\cos(\omega_0 t)}{r}, \qquad B_\theta=\frac{E_0\cos(\omega_0 t)}{r}, \tag{3}$$

where $E_0=V_0\ln(r_0/r_i)$ and V_0 is the voltage across the inner and outer conductors of the coaxial line, and ω_0 is the frequency. The power carried by the TEM wave is given by

$$P=\frac{c}{4\pi}\int \mathbf{E}\times\mathbf{B}\cdot d\,\mathbf{A} =\frac{c}{2}E_0^2\ln\left[\frac{r_0}{r_i}\right]\cos^2(\omega_0 t) . \tag{4}$$

The time-averaged power is

$$\langle P\rangle=\frac{c}{4}E_0^2\ln\left[\frac{r_0}{r_i}\right] . \tag{5}$$

In our simulations, probes are placed at various axial positions inside the waveguide to monitor the power flow as a function of time. The axial positions where the Poynting vector is calculated across the cross-sectional area of the waveguide are indicated by arrows in Fig. 1. Figure 2 shows typical results of the power probes from a simulation in which a TEM mode with a trapezoidal pulse shape was launched. The transmission coefficient can then be obtained by taking the ratio between the incoming and outgoing microwave power levels. The results of the transmission coefficient from a set of simulations with different microwave frequencies are shown in Fig. 3. The parameters for the simulations were $r_0=7.62$ cm, $r_i=2.54$ cm, the aperture gap $\Delta=1.0$ cm, and the length of the aperture $l=1.0$ cm. The lowest cutoff frequency for higher-order TM waves is $f_{co}=c/2\Delta=2.95$ GHz. In this case study, the transmission coefficient showed a monotonically decreasing behavior as the frequency was increased. The transmission coefficient de-

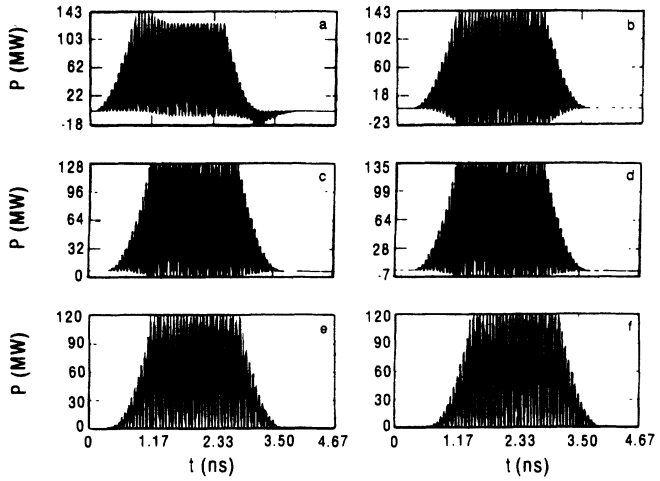

FIG. 2. Typical microwave power measurements at different axial positions in the computer simulations.

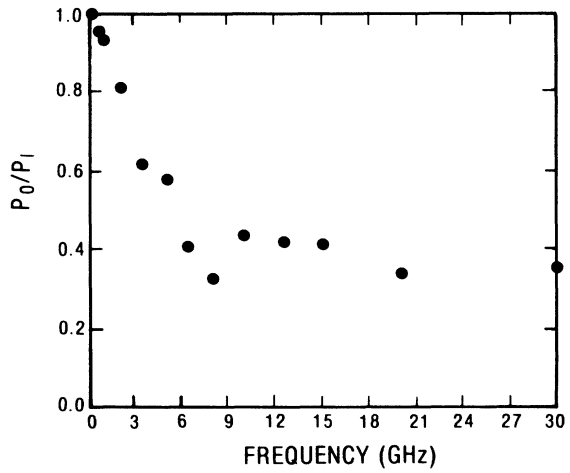

FIG. 3. Microwave transmission coefficient as a function of microwave frequency as obtained from computer simulations.

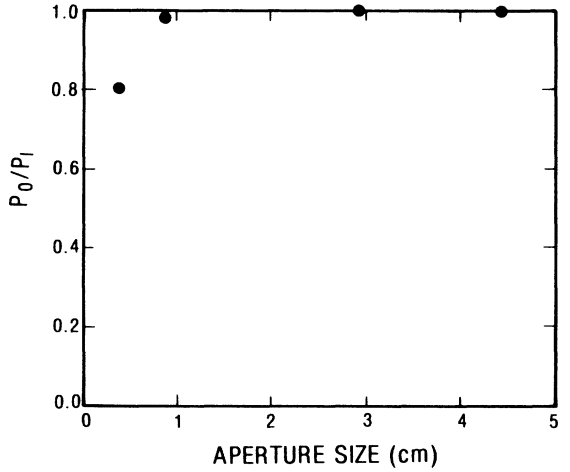

FIG. 4. Microwave transmission coefficient as a function of aperture size for the case with microwave frequency of 0.2 GHz.

creased sharply until the frequency of the microwave reached about f_{co}. Then the fraction of power transmitted through the aperture approached an asymptotic value of 35%. The rest of the microwave power was observed as a reflected wave.

It is evident from Fig. 3 that low-frequency microwaves have better transmission properties. Another interesting characteristic shown by the simulations is that the length of the aperture had only a small effect in the transmission of microwave power at a fixed frequency. For example, the length of the aperture was varied from 0.5 to 6.0 cm at a frequency of 10 GHz and the transmission coefficient only changed from 45% to 25%.

On the other hand, the size of the aperture can be an important factor in microwave transmission, depending on the microwave frequency. Figure 4 shows the transmission coefficient as a function of the aperture size at a microwave frequency of 0.2 GHz. The results in Fig. 4 show that it does not strongly depend on the aperture size and, in fact, it is rather constant until the aperture becomes very small. Even with the smallest aperture, 80% of the microwave power can still be transmitted through. However, this is not true for higher-frequency microwaves. In Fig. 5, we show the transmission coefficient of microwaves of frequency $f=6.5$ GHz, and the strong dependence on the aperture size is evident. When the aperture was 90% open, the power transmission was almost perfect ($\eta=92\%$). But as the size of the aperture decreases, the efficiency of power transmission decreases rapidly in almost a linear manner. One can explain the behavior by considering the excitation of higher-order modes and its nature. Higher-order modes are excited at the boundaries of the aperture to satisfy the boundary conditions; however, these modes can be either propagating through or decaying away from the aperture, depending upon whether the frequency of the incident microwaves is above or below the cutoff frequency of 2.95 GHz given by Eq. (1). When the frequency is well below cutoff, as it was in the case of Fig. 4, the higher-order TM modes are necessarily evanescent and, therefore, the microwave power was primarily in the fundamental TEM mode which has no cutoff. Consequently, the power can be efficiently transmitted thought the aperture irrespective of the size of the aperture.

The pulse length of the incident microwave can also be important in its transmission throughout the aperture in the linear regime. Our simulations show that the transmission coefficient rises to an asymptotic limit as the pulse length increases. The asymptotic limit is, of course, determined by the geometry of the waveguide and the microwave frequency as shown in Figs. 2–4. In Fig. 6, we show the transmission of a microwave pulse of various duration at a frequency of $f=6.5$ GHz through the apertured coaxial waveguide. The microwave pulse assumes a trapezoidal shape with a 3.3-ps rise and fall time. The pulse length is the flat top of the pulse. As the pulse length becomes short, the transmission coefficient diminishes. A significant fraction of the power is reflected. This phenomenon is clearly illustrated in Fig. 7 from a simulation of the transmission of a microwave pulse with a pulse length of $\frac{1}{3}$ ns, where the time history of the axial Poynting flux showed strong reflection. The behavior can

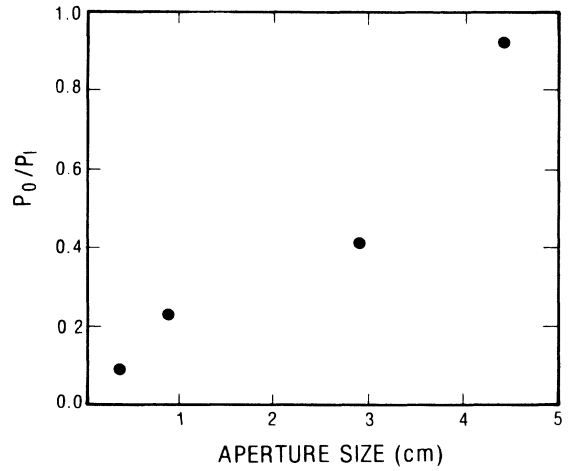

FIG. 5. Microwave transmission coefficient as a function of aperture size for the case with microwave frequency of 6.5 GHz.

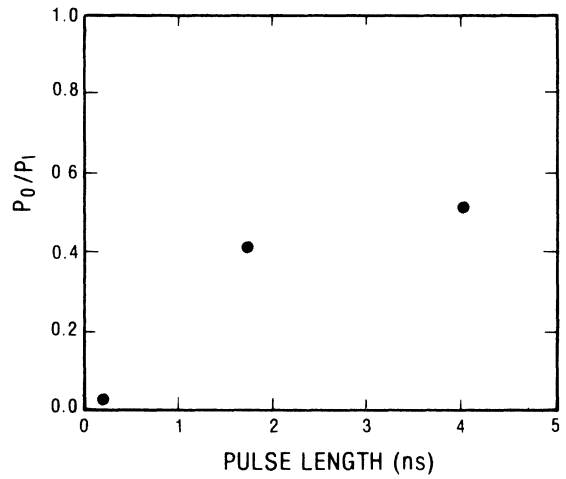

FIG. 6. Microwave transmission coefficient as a function of pulse length for the microwave frequency of 6.5 GHz.

be understood in the following way. For a finite pulse, the continuous-wave train approximation is not valid and the microwave power is distributed among various frequencies. The low-frequency component can be transmitted relatively efficiently, however, the high-frequency component is mostly reflected. In a short-pulse situation, the power is concentrated in the high-frequency component and, therefore, the power transmission is low.

In a general approach, the apertured waveguide can be analyzed as a circuit consisting of capacitors and inductors. The impedances of the circuit elements depend on geometric parameters and in a time-varying (ac) situation they are also frequency dependent. The resultant impedance representing the aperture can exhibit resonances with the incident microwave frequency. Significant transmission of microwave power can occur at resonances. In order to show this effect, we performed another set of simulations with different geometric parameters ($r_i = 0.635$ cm, $r_0 = 1.905$ cm, $\Delta = 1.8128$ cm, and $l = 1.0$ cm). The lowest cutoff frequency for the higher-order TM waves is $f_{co} = c/2\Delta = 11.81$ GHz. The transmission coefficient as a function of microwave frequency is shown in Fig. 8. The low-frequency microwaves can be transmitted through the aperture very well and in general the transmission starts to decline as the frequency is increased. However, in our simulations we observed anomalous transmission near resonances for high-frequency microwaves as illustrated in Fig. 8.

III. NONLINEAR REGIME

In the nonlinear regime where electron emission can occur, the physics is more complicated. Aperture closure is now possible due to electron flow across the gap, an effect which can be further greatly enhanced by secondary electron emission. This secondary emission can cause permanent breakdown of the transmission line structure if it is in phase with the driving TEM field. This avalanche effect, called multipacting,[5] is a problem in many rf structures, but can usually be avoided by increasing the electric field rapidly over the multipacting limit, or by electrode surface coatings,[6–9] which have recently proven to be quite successful.

To estimate the closure phenomena due to field emission, consider electrons emitted off a section of the aperture (Fig. 1). If we approximate the problem to be one-dimensional in the radial direction, then the equation of an electron with charge $q = -e$ emitted off a conducting boundary assumed to be at $r = 0$ is

$$\frac{dp}{dt} = qE_0 \sin\omega t \ , \tag{6}$$

where $p = \gamma mv$ is the particle momentum, E_0 is the TEM electric field amplitude, and ω is the TEM frequency. If the particle is born with zero initial velocity at a time t_0 into the emission cycle, the solution to this equation is[10]

$$\gamma v = (qE_0/m\omega)(\cos\omega t_0 - \cos\omega t) \ . \tag{7}$$

The position $r = r(t)$ of the particle is then

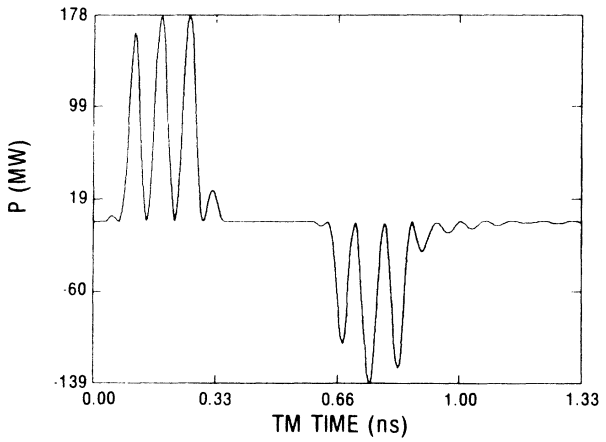

FIG. 7. Significant reflection of microwave power of short-pulse duration was observed in computer simulations.

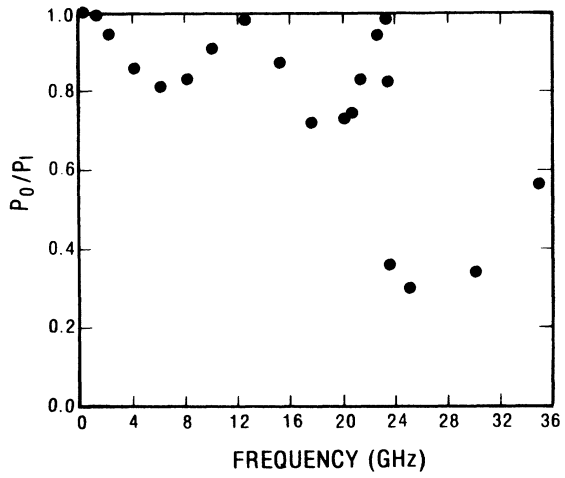

FIG. 8. Transmission coefficient of microwaves showed resonant behavior with frequency.

$$r(\tau,\tau_0)=\left[\frac{\alpha c}{\omega}\right]\int_{\tau_0}^{\tau}d\tau(\cos\tau_0-\cos\tau)/[1+\alpha^2(\cos\tau_0-\cos\tau)^2]^{1/2}\ , \tag{8}$$

where $\alpha=qE_0/m\omega c$ and $\tau=\omega t$. For the particle to reach the other side of the aperture, the distance traveled should be greater than the aperture spacing Δ. In the nonrelativistic ($\alpha \ll 1$) case, this gives the condition[10]

$$2\sin\tau_0+2(\pi-t_0)\cos\tau_0>m\omega^2\Delta/qE_0\ . \tag{9}$$

Note that the initial burst of particles emitted at $t_0=0$ will reach the other side if $m\omega^2\Delta/qE_0<2\pi$. Hence aperture closure in the nonrelativistic case can be avoided by choosing a high enough frequency or low enough wave amplitude such that $m\omega^2\Delta/qE_0>2\pi$. Physically, this corresponds to either reversing the phase of the TEM wave before the particle traverses the gap, or decreasing the field strength so that the particle is unable to reach the opposite electrode before the phase reverses.

The more general condition for aperture closure can be determined from Eq. (8). An initial burst of particles emitted at a time $t_0=0$ will cross the gap if

$$\Delta<\left[\frac{\alpha c}{\omega}\right]\int_0^{\tau}dt\,(1-\cos\tau)/[1+\alpha^2(1-\cos\tau)^2]^{1/2}\ . \tag{10}$$

To further analyze the problem of microwave propagation, and to provide a benchmark for the theoretical analysis, $2\frac{1}{2}$-dimensional relativistic and fully electromagnetic plasma simulations were done with the particle-in-cell code ISIS. The surfaces of the apertured section in Fig. 1 were allowed to emit electrons if the normal electric field was above a field-emission threshold of 50 kV/cm. TEM waves of frequency ω and amplitude E_0 were propagated down the transmission line from the left-hand side of the simulation region; probes measuring the magnitude of the Poynting vector integrated over the cross-sectional area were placed throughout the simulation region. A probe near the exit to the simulation box was used to measure the transmitted power; the transmitted power $P_{\rm tr}$ was then normalized to incident power P_0. The ratio $P_{\rm tr}/P_0$ was investigated for different frequencies and incident microwave power; the aperture size of 2.95 cm was held constant in these runs.

The simulations demonstrate that with field emission enabled, electrons may cross the gap if the electric field is large enough for a given frequency (Fig. 9). The resulting emission can essentially close the gap, and thus decrease $P_{\rm tr}/P_0$. A measure of this electric field strength can be conveniently described by the nondimensional ratio Ω/ω, where $\Omega=eE_0/mc$. In Fig. 10 we show simulation measurements of $P_{\rm tr}/P_0$ versus Ω/ω for two different frequencies, 500 MHz and 2 GHz. Note that both curves seem to scale approximately the same and show significant improvement in microwave transmission for values of $\Omega/\omega>10$. That is, the gap closure is no longer effective, and microwave transmission greatly improves. The deviation bars in the figure are primarily due to a beating phenomenon in the oscillating magnitudes of $P_{\rm tr}/P_0$ over alternating cycles (Fig. 11). The lower and upper parts of the deviation bar correspond to the minimum and maximum of the probe traces, and the data point itself corresponds to the average of these two values.

Note that in both our analysis and the simulations, we have assumed that the electric field strength in the aperture is below voltage breakdown levels. This may not be true for the higher values of Ω/ω shown in Fig. 10. At lower frequencies, the gap should reopen at lower field strengths than the voltages shown in Fig. 10. Typically, voltage breakdown in 3-GHz cavities is around 240 MV/m,[11] although recent electrode surface studies report an improvement in voltage holdoff by around 50% by the use of CaF_2 coatings.[9] In addition, the presence of the strong transverse magnetic field B_θ for large TEM wave amplitudes may also increase the voltage holdoff levels.

The reopening of the aperture as demonstrated in Fig. 10 is an interesting phenomenon. It is due to a large $\mathbf{E}\times\mathbf{B}$ force in the aperture which sweeps the electrons downstream, preventing the electrons from crossing the gap. This is similar to magnetic insulation in high-current electron diodes, where the insulation is more efficient at higher field strengths. To investigate the physics of the gap reopening more carefully, consider the general (nonrelativistic) equations of motion for a particle with charge $q=-e$ in a coaxial structure,

$$\frac{d}{dt}(\gamma v_z)=\frac{q}{m}(E_z+v_rB_\theta/c)\ , \tag{11a}$$

$$\frac{d}{dt}(\gamma v_r)=\frac{q}{m}(E_r-v_zB_\theta/c)\ . \tag{11b}$$

We will neglect the self-fields of the emitted particles, so that $\mathbf{E}$ and $\mathbf{B}$ are due exclusively to the TEM wave. In the fundamental mode, $E_z=0$, and $E_r=B_\theta$, so that Eqs. (11) become

$$\frac{d}{dt}(\gamma v_z)=\frac{q}{m}(v_rB_\theta/c)\ , \tag{12a}$$

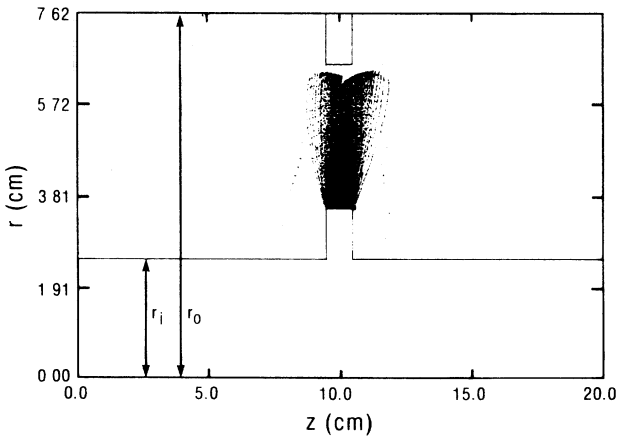

FIG. 9. Simulation snapshot of particle emitted off lower aperture surface being accelerated towards top electrode.

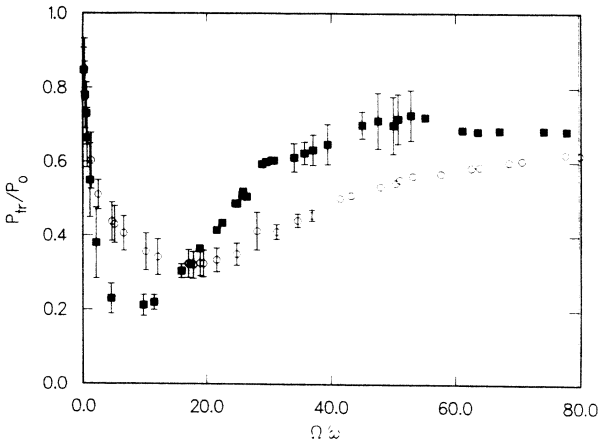

FIG. 10. Plot of P_{tr}/P_0 vs Ω/ω for two different values of frequency, 500 HMz (open circles) and 2 GHz (closed squares). The 500-MHz simulations also have a three-times longer pulse length. Note the similarity in the two curves and the reopening of the gap for $\Omega/\omega > 10$.

$$\frac{d}{dt}(\gamma v_r) = \frac{q}{m} B_\theta (1 - v_z/c) \ . \tag{12b}$$

As a first approximation, consider Eqs. (12) in the nonrelativistic limit that v_r/c and $v_z/c \ll 1$. In that case we have

$$\frac{dv_z}{dt} = \frac{q}{m}(v_r B_\theta / c) \ , \tag{13a}$$

$$\frac{dv_r}{dt} = \frac{q}{m} B_\theta \ . \tag{13b}$$

In the nonrelativistic limit, the magnetic field terms B_θ can be eliminated from Eqs. (13) to yield a constant of motion. Solving for qB_θ/mc from Eq. (13a) and substituting into Eq. (13b) yields

$$v_r \frac{dv_r}{dt} = c \frac{dv_z}{dt} \ . \tag{14}$$

Or, $v_z = v_r^2/2c$. There are two important facts from this relation. First, no matter what the sign of v_r, v_z is always positive. Hence particles emitted from either electrode are always accelerated in the same direction, i.e., downstream from the gap. This is observed in the simulations. Second, v_z is always less than v_r, as one would expect in the nonrelativistic case.

Consider now a TEM wave of amplitude V_0 in a coaxial waveguide of inner and outer radii r_1 and r_2, respectively. We have

$$B_\theta(r,t) = E_r(r,z,t) = \frac{V_0}{r \ln(r_2 r_1)} \exp i(kz - \omega t) \ . \tag{15}$$

If r_1 and $r_2 \gg \Delta$ and $kl < 1$, where Δ and l are the size and length of the gap, the amplitude of the TEM wave within the gap is a weak function of r and z. With the proper choice of phasing, we can then write $B_\theta(r,t) = B_0 \sin\omega t$, where B_0 depends only weakly or r and z but is a direct measure of the TEM wave amplitude. Equations (13) then become

$$\frac{dv_z}{dt} = \frac{q}{m}(v_r B_0/c)\sin\omega t \ , \tag{16a}$$

$$\frac{dv_r}{dt} = \frac{q}{m} B_0 \sin\omega t \ . \tag{16b}$$

If $\Omega = qB_0/mc$, the solution to Eq. (16b) for a particle emitted at a time t_0 into the cycle is

$$\frac{v_r}{c} = \frac{\Omega}{\omega}(\cos\omega t_0 - \cos\omega t) \ , \tag{17}$$

in agreement with Eq. (7). However, in this more general case there is now an axial component to the electron motion given by Eq. (16a),

$$\frac{dv_z}{dt} = \frac{\Omega^2 c}{\omega} \sin\omega t (\cos\omega t_0 - \cos\omega t) \ . \tag{18}$$

This is easily integrated to give

$$\frac{v_z}{c} = \frac{\Omega^2}{2\omega^2}(\cos\omega t_0 - \cos\omega t)^2 \ , \tag{19}$$

in agreement with Eq. (21). Clearly, our assumption $v_z/c \ll 1$ holds if $\Omega^2/\omega^2 \ll 1$, or since $\alpha = qE_0/m\omega c = \Omega/\omega$, $\alpha^2 \ll 1$. For large TEM wave amplitudes (or, equivalently, low frequencies) such that $\Omega^2/\omega^2 \gtrsim 1$, the nonrelativistic limit in our equations is not applicable, and we need to solve Eqs. (12) exactly.

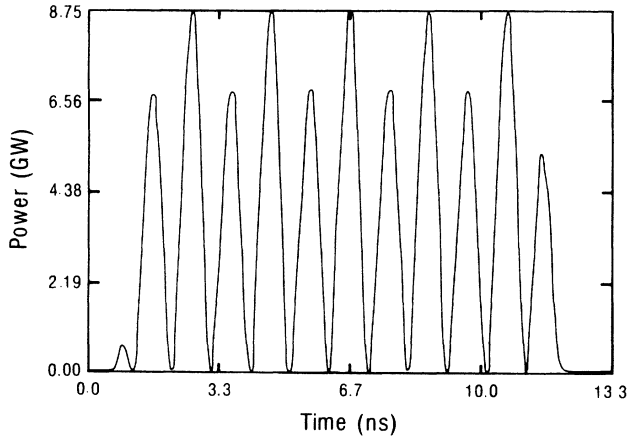

FIG. 11. Oscillating magnitudes of measured power in the downstream Poynting probe for a simulation with $\Omega/\omega = 4.7$. The variations over the alternating cycles are responsible for the deviation bars in some of the data points pictured in Fig. 10.

IV. GENERAL SOLUTION

In terms of the fully relativistic conjugate momenta, $p_r = \gamma m v_r$ and $p_z = \gamma m v_z$, Eqs. (12) can be written

$$\frac{d}{dt} p_z = \Omega \frac{p_r}{\gamma} \sin\omega t \ , \tag{20a}$$

$$\frac{d}{dt}p_r=\Omega mc(1-p_z/\gamma mc)\sin\omega t \ . \tag{20b}$$

If we define a new independent variable by $dx=\sin\omega t d(\omega t)$, then $x=\cos\omega t_0-\cos\omega t$, and Eq. (18) becomes

$$\frac{dp_z}{dx}=\frac{\Omega}{\gamma\omega}p_r \ , \tag{21a}$$

$$\frac{dp_r}{dx}=\frac{\Omega}{\gamma\omega}(\gamma mc-p_z) \ . \tag{21b}$$

Multiplying Eq. (21a) by p_z and Eq. (21b) by p_r, and adding the two equations, yields

$$p_r=\frac{1}{2}\left[\frac{\omega}{\Omega mc}\right]\frac{d}{dx}(p_r^2+p_z^2) \ .$$

Using $p_r=(\gamma\omega/\Omega)dp_z/dx$ from Eq. (21a) gives

$$\frac{dp_z}{dx}=\left[\frac{mc}{2\gamma}\frac{d}{dx}\right]\left[\left[\frac{p_r}{mc}\right]^2+\left[\frac{p_z}{mc}\right]^2\right]$$

$$=mc\left[\frac{d\gamma}{dx}\right] ,$$

since $\gamma=[1+(p_r/mc)^2+(p_z/mc)^2]^{1/2}$. Hence

$$\frac{d}{dx}(p_z-\gamma mc)=0$$

or, integrating and using the initial condition that $p_z=0$ at $t=t_0$ (i.e., $x=0$) gives $p_z=(\gamma-1)mc$. Substituting this in Eq. (21b), we get

$$\frac{dp_r}{dx}=\frac{\Omega}{\gamma\omega}mc \ . \tag{22}$$

If we now combine this with Eq. (21a) we find that

$$\frac{p_z}{mc}=\frac{1}{2}\left[\frac{p_r}{mc}\right]^2 , \tag{23}$$

and substituting this into γ in Eq. (22) gives

$$\frac{dP}{dx}=\pm\frac{2\Omega}{\omega}\frac{1}{P^2+2} , \tag{24}$$

where $P\equiv p_r/mc$, and we choose the sign in Eq. (24) according to the particular cycle of the wave. That is, during the (accelerating) first half-cycle, $dp_r/dx>0$, and during the following (decelerating) half-cycle, $dp_r/dx<0$. Hence, upon integration, we obtain a cubic equation for P in terms of x,

$$P^3+6P-6(\Omega/\omega)x=0 \ .$$

The only real root of this equation is given by

$$P=\left[\frac{3\Omega}{\omega}x\right]^{1/3}(A^++A^-) , \tag{25}$$

where

$$A^{\pm}=\left[1\pm\left[1+\frac{8}{9}\frac{\omega^2}{\Omega^2x^2}\right]^{1/2}\right]^{1/3} . \tag{26}$$

Equations (23) and (25) are the general solution to our problem. Note that for $\Omega^2/\omega^2\ll1$, these equations reduce to the nonrelativistic solutions, Eqs. (16) and (19).

The more interesting case arises for large TEM wave amplitudes such that $\Omega^2/\omega^2\gg1$. In this case the solution becomes (for $x\neq0$)

$$v_r/c=2(6\Omega/\omega x)^{-1/3}\rightarrow0$$

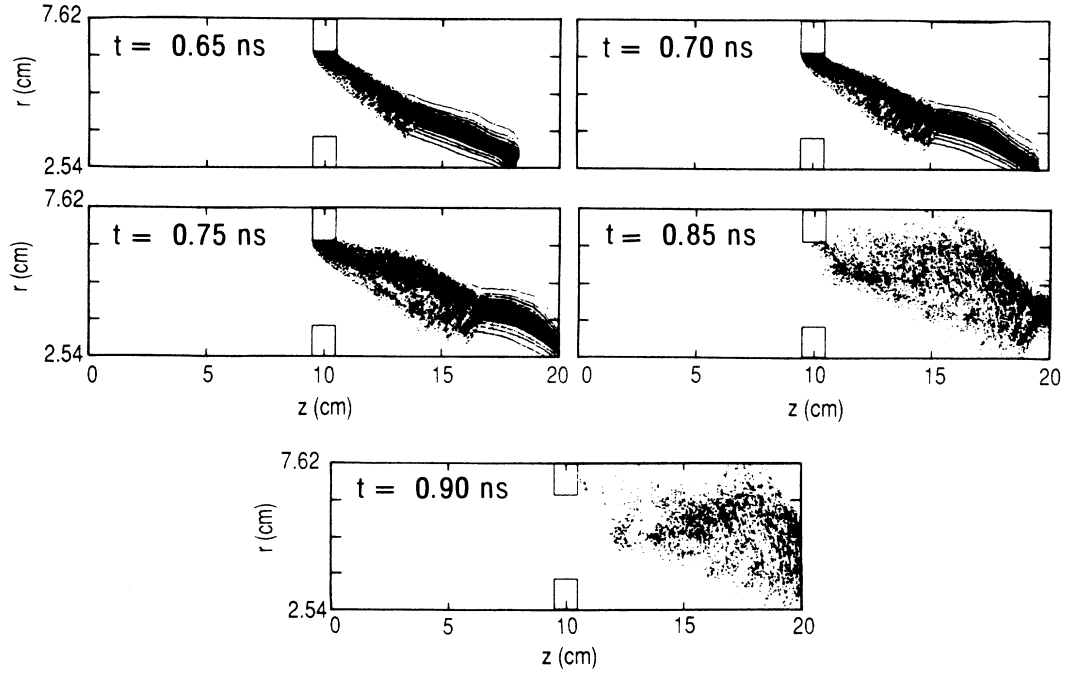

FIG. 12. Typical simulation snapshots of particles emitted at the top aperture surface for $\Omega/\omega>40$. Instead of closing the gap the plasma is turned back by magnetic forces, and is carred along downstream.

and

$$v_z/c \rightarrow 1 \ .$$

Hence, for large TEM wave amplitudes, $v_z \rightarrow c$. The emitted electrons are then seen to $\mathbf{E}\times\mathbf{B}$ drift down the coaxial structure, and since the radial velocity component $v_r \rightarrow 0$, gap closure cannot occur. In Fig. 12, a series of simulation snapshot's at various times is shown, showing the blowoff of the current across the gap as the field strength is increased within a field cycle. This blowoff manifests itself in a large axial electron velocities and decreased radial velocities, so that the aperture reopens.

Our simple model, Eqs. (20), predicts that the ratio Ω/ω is the critical parameter defining the two regions for which the aperture is either open or closed. In Fig. 10 we plotted the ratio of transmitted to incident power versus Ω/ω for different wave amplitudes and frequencies. The results of the simulations indicate that the physics in the nonlinear regime can be described quite adequately by the ratio Ω/ω alone. The reopening of the aperture at higher TEM amplitudes ($\Omega/\omega > 10$) scales somewhat differently for each frequency because magnetic insulation is always more efficient at higher field strengths. Hence, for a fixed value of Ω/ω, the ratio $P_{\rm tr}/P_0$ should always be greater for larger field strengths, and thus higher frequencies. For frequencies above cutoff (in these simulations, about 3 GHz), higher-order modes can propagate in the structure, and this scaling may not be obeyed, because the driving fields may be distinctly different from those assumed in Eqs. (20). In Fig. 13 we plot simulation data of the ratio $P_{\rm tr}/P_0$ versus Ω/ω for 2-GHz and 4-GHz incident microwave radiation. For the 4-GHz simulations the gap never reopens but remains closed. Because higher-order modes are now important, the simple $\mathbf{E}\times\mathbf{B}$ phenomenon demonstrated in the analysis of the fundamental mode is no longer applicable. It is thus necessary to drive the coaxial wave guide at frequencies below cutoff for the gap to reopen.

In the fundamental TEM mode, our simple model does not include spatial variations of the TEM wave within the gap [e.g., the $1/r$ dependence in Eq. (15)], and does not take into account the self-fields of the particles, though this is obviously important for relativistic velocities. Nevertheless, it has been shown that the simple Ω/ω scaling model developed in this section is helpful in understanding the nonlinear effects taking place within the aperture, and can act as a firm foundation upon which to build in later studies.

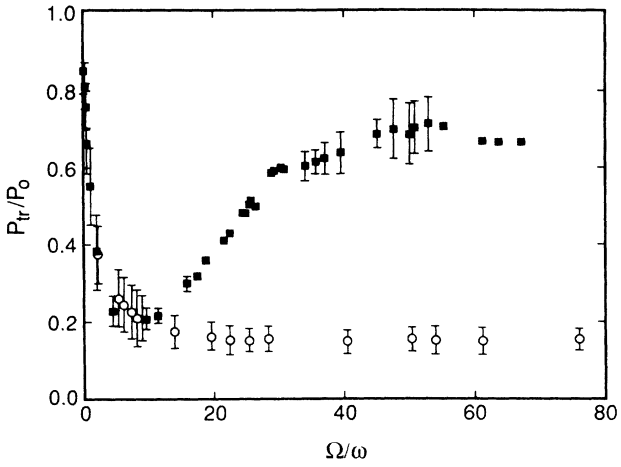

FIG. 13. Plot of $P_{\rm tr}/P_0$ vs Ω/ω for 2 GHz (closed squares) and 4 GHz (open circles). Because 4 GHz is above cutoff, the magnetic insulation calculation given in the text is not applicable. Hence, the aperture closes for large TEM amplitudes, and does not reopen as in the 2-GHz case.

V. CONCLUSIONS

In the linear regime, we showed that low-frequency microwaves (<1 GHz) can be efficiently transmitted through an apertured coaxial structure. However, the transmission coefficient decreases as the frequency of the microwaves increases. When the effective impedance resonates with the frequency of the incident microwaves, anomalous power transmission can occur. We also showed the effects of aperture size and microwave pulse length on the power transmission. The results from our study indicate that favorable microwave power transmission occurs in the low-frequency regime and for high-frequency microwave transmission one might have to take advantage of the resonance feature of the equivalent circuit.

In the nonlinear regime where field emission of electrons can occur, we showed that the important characteristic parameter is Ω/ω. Efficient power transmission can occur in two regions, namely, $\Omega^2/\omega^2 \ll 1$ and $\Omega^2/\omega^2 \gg 1$. When $\Omega^2/\omega^2 \ll 1$, the field-emitted electrons would not cause significant gap closure because the effective transverse excursion is small. As for $\Omega^2/\omega^2 \gg 1$, the amplitude of the TEM wave is large enough for magnetic insulation to occur and, therefore, the aperture gap will be reopened. In most practical situations, the parameter regime where $\Omega^2/\omega^2 \ll 1$ would apply for effective transmission of microwave power when field emission of electrons occurs. For fixed microwave power, one can achieve this condition simply by raising the frequency.

ACKNOWLEDGMENTS

We wish to acknowledge a helpful discussion with Dr. A. L. Peratt and Dr. W. R. Shanahan. This work was supported by the U. S. Department of Energy.

[1]G. R. Gisler and M. E. Jones, Bull. Am. Phys. Soc. **29**, 1208 (1984).

[2]C. C. Johnson, *Field and Wave Electrodynamics* (McGraw-Hill, New York, 1965), p. 142.

[3]S. Silver, *Microwave Antenna Theory and Design* (Dover, New York, 1965), p. 217.

[4]J. R. Whinnery and H. W. Jamieson, Proc. IRE **32**, 98 (1944); J. R. Whinnery, H. W. Jamieson, and T. E. Robbins, Proc. IRE **32**, 695 (1944).

[5]E. W. B. Gill and A. von Engel, Proc. R. Soc. London, Ser. A **192**, 446 (1948).

[6]W. Peter, J. Appl. Phys. **56**, 1546 (1984).

[7]D. Ruzic, R. Moore, and D. Manos, and S. Cohen, J. Vac. Sci. Technol. **20**, 1313 (1982).

[8]R. W. Beirec, J. Jasber, and J. V. Labacqz, in *The Stanford Two-Mile Accelerator,* edited by R. B. Neal (Benjamin, New York, 1968), Chap. 10.

[9]J. N. Smith, Jr., J. Appl. Phys. **59**, 283 (1986).

[10]W. Peter, R. J. Faehl, and M. E. Jones, Part. Accel. **21**, 59 (1982).

[11]E. Tanabe, IEEE Trans. Nucl. Sci. **NS-30**, 3551 (1983).

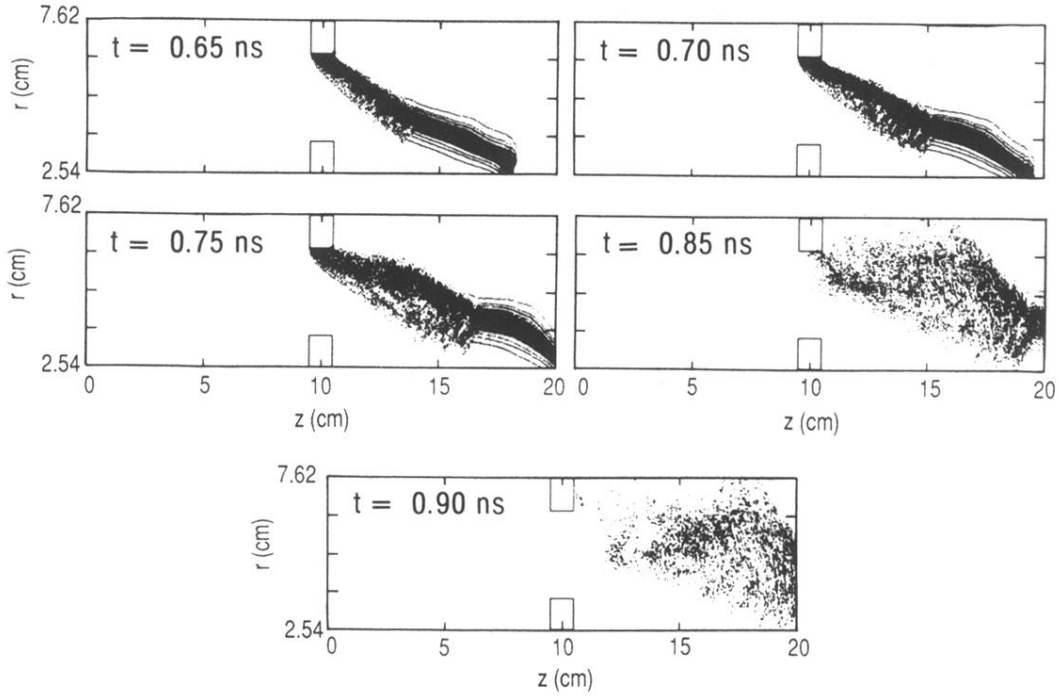

FIG. 12. Typical simulation snapshots of particles emitted at the top aperture surface for $\Omega/\omega > 40$. Instead of closing the gap the plasma is turned back by magnetic forces, and is carred along downstream.

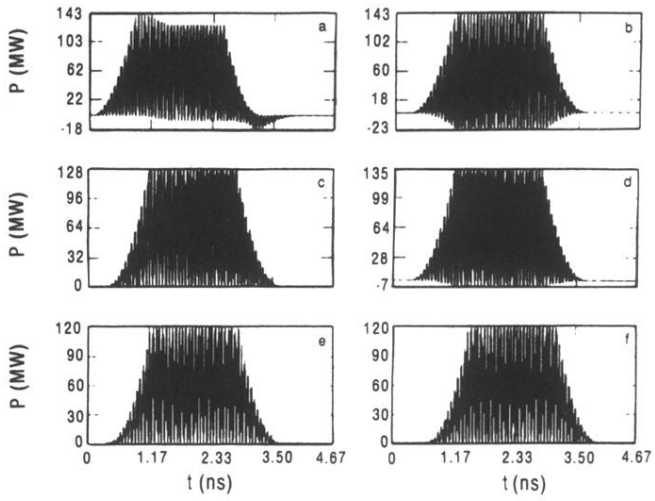

FIG. 2. Typical microwave power measurements at different axial positions in the computer simulations.

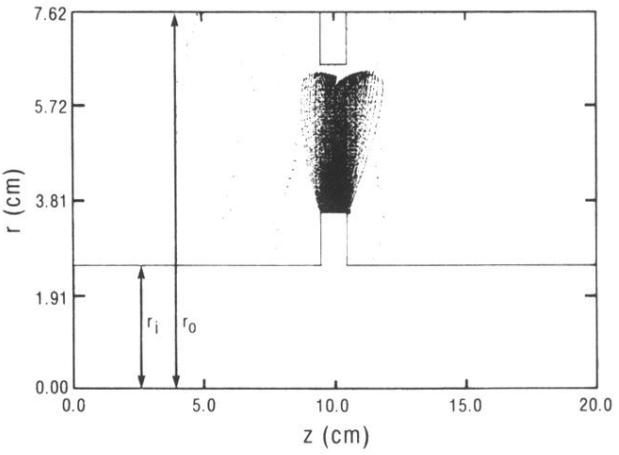

FIG. 9. Simulation snapshot of particle emitted off lower aperture surface being accelerated towards top electrode.